Thermal spike effects in low-energy single-ion impacts on graphite

Q. Yang,* T. Li, B. V. King, and R. J. MacDonald
Department of Physics, The University of Newcastle, NSW 2308, Australia
(Received 28 August 1995)

Monte Carlo simulations have been used to obtain three-dimensional distributions of cascade defects and energy deposition due to single-ion impacts in graphite. This energy deposition profile serves as the starting point for the formation and evolution of the thermal spike. In this case the minimum deposited energy density per target atom for the spike formation is the order of the atomic binding energy. An effective spike created by a single-ion impact in the near-surface region is introduced to account for the bump formation on the highly oriented pyrolytic graphite surface. A linear relationship between the bump volume and the effective spike energy is obtained based on the thermal spike model, which agrees well with the scanning tunnel microscope results. It is suggested that the one-dimensional energy deposition rate dE/dx is not suitable to describe spike effects. On the other hand, a three-dimensional parameter corresponding to the nature of the spike formation should be used.

I. INTRODUCTION

The interaction of energetic particles with solids and surfaces has been an area of great research interest for both fundamental studies and material applications. The collision processes and phenomena have been studied extensively.[1–4] Recently, computer simulations have become useful tools in studying the collision processes of ions in solids while conventional theories provide analytic expressions and guidelines.[4–7] Normally, the linear cascade theory has been used to estimate the damage production in solids due to ion bombardment.[4,5] On the other hand, spikes effects have been discussed in early articles,[1,2] and have been used to explain the nonlinear effects observed in sputtering experiments recently.[8,9] However, detailed microscopic mechanisms in the collision processes are not yet fully understood. Recent studies with the scanning tunneling microscope[10–16] (STM) and molecular-dynamics (MD) simulations[17–22] for the effects of single-ion impacts on surfaces have however brought insight into the cascade processes on the atomic scale. Craters have been found around the point of impact of keV ions on various material surfaces and interfaces,[10] while only bumps have been observed on graphite surfaces.[11–16] A relaxation model based on the defect distributions obtained from Monte Carlo simulations has been used to predict the formation of craters on some solid surfaces.[23] MD simulations of low-energy Au bombardment of Au have demonstrated the formation of thermal spikes which lead to local melting and viscous flow in the formation of surface damage.[21] However, the actual mechanisms for the formation of bumps on graphite are not fully understood. Recently, the thermal spike effect has been discussed in the STM studies of bump formation by keV ion bombardment of highly ordered pyrolytic graphite (HOPG).[14,16] Various models have been discussed in more detail,[16] in which it is suggested that thermal spikes created by low-energy ions in the near-surface region play an important role in producing the surface bumps. Generally, thermal spike effects dominate for low-energy heavy ion irradiation while other processes dominate for light ion impact where no significant spike effects take place.[1,16,24] MD simulations of 500 eV C bombardment of HOPG indicate that surface bumps are formed due to defect stresses developed by the collision cascade in the near-surface layers of the target,[22] while STM observations reveal point defect formation due to 50 eV Ar bombardment of HOPG surface.[15]

In the previous study,[16] the three-dimensional distribution of deposited energy has been obtained using a modified Monte Carlo TRIM code (TRIM3D). This energy deposition profile serves as the starting point for the formation and evolution of the thermal spike. It is found that the average bump volume observed on HOPG surfaces scales linearly with the effective spike energy in the near-surface region. The thermal spikes created by single-ion impacts in the near-surface region are believed to be responsible for the bump formation on HOPG surface in the cases studied.[14,16] However, no explanation is given for the linear relationship between the bump volume and the effective spike energy. Also, no spike component is predicted for 20 keV N^+ bombardment of HOPG although bumps have been observed.[14] The later is because that the average energy density used in the previous study[16] was based on an average profile of energy deposition over large number of ion histories relative to the impact point on the surface. The resulted energy density was smeared laterally due to the statistical spread of the ion trajectories, which is not suitable for single-ion impact events.

In this study, the TRIM3D code has been further modified as described in the next section. The average energy density is calculated relative to the ion trajectory as a function of depth. The influence of ion trajectories on the statistical profile of energy deposition can be eliminated in this way, thus the resulted energy density should be suitable for single-ion impacts. This correction is found most significant for the case of 20 keV N^+ bombardment, for which spike effects are expected in this study. In addition, by considering the local deformation of an effective hot zone due to the spread of the spike energy, a linear relationship between the bump volume and the effective spike energy is derived, which agrees well with the STM results. It is suggested that the one-dimensional energy deposition rate dE/dx is not suitable to

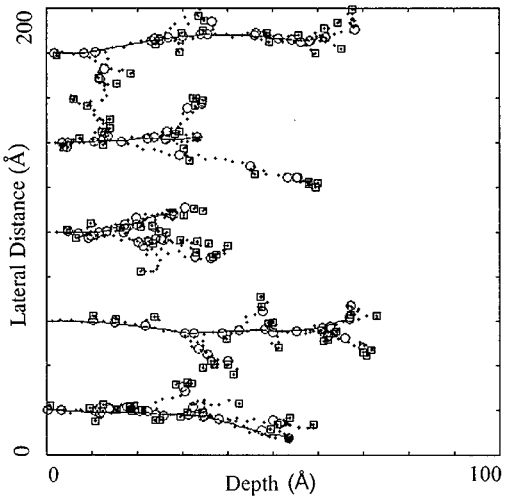

FIG. 1. Five typical cascades of 3 keV Ar^+ ions at normal incidence into graphite. —ion trajectory, ○ vacancy, □ interstitial, + phonon.

describe spike effects. On the other hand, a three-dimensional parameter corresponding to the nature of spike formation should be used.

II. CASCADE AND ENERGY DEPOSITION DUE TO SINGLE-ION BOMBARDMENT

The passage of an energetic ion through a solid leaves a track of cascades surrounding its trajectory, where defects (vacancies, interstitials, phonons, etc.) are created. A detailed description for such a process can be found in Ref. 4, and the binary collision processes can be simulated by Monte Carlo methods such as TRIM (Ref. 4) or MARLOWE.[7] The energy deposited into the nuclear process mainly contribute to the local vibration of lattice atoms via the production of phonons. In order to obtain the three-dimensional distribution of these defects and energy deposition by a single-ion impact, a PC code TRIM'89 (Ref. 4) has been modified (TRIM3D) to trace the production of each defect. It has been suggested that electronic energy straggling should be considered in the calculation of energy deposition profile.[9] In the current TRIM3D code, electronic energy straggling is included[26] using the empirical formula.[27,28] In the simulations, the graphite target is treated as amorphous with a density of 2.26 g/cm^3.[4,29] The production of defects depends upon the displacement energy,[4] which is chosen to be 35 eV for graphite.[30] The surface binding energy is taken to be the sublimation energy, 7.41 eV.[4] The cutoff energy for following particles in the cascades is chosen as 2 eV [typically about 1–2 eV (Ref. 4)], while the simulated energy distribution is not sensitive to this value. Figure 1 illustrates five typical cascade histories of 3 keV Ar^+ ions in graphite. It is seen that most of the defects are located surrounding the ion trajectory although the details of the cascades may differ very much from each other. In order to obtain statistical generality, it is suitable to take the average over large numbers of ion histories. For the case of single-ion impacts, the averaging procedure is described below.

During the passage of each ion in the target, the ion trajectory and the positions of all the defects created are stored. After the cascade due to this ion completes, the distribution of the defects created by this ion is calculated relative to the ion trajectory laterally as a function of depth. Such a procedure repeats for large numbers of ion histories for enough statistics, and the final distribution of defects surrounding the ''average'' single-ion trajectory is obtained. For example, Fig. 2 shows the average distribution of vacancies, interstitials and phonons around a 3 keV Ar^+ trajectory in graphite. It should be pointed out that the lateral dimension is relative to the ion trajectory while each ion trajectory is not necessarily a straight line as shown in Fig. 1. On an average, Figs. 2(a) and 2(b) clearly display the formation of a displacement spike which consists of a shell of interstitial atoms surrounding a core of vacancies during the ballistic phase.[2,10,21] However, most of the vacancies and interstitials are distributed within a few angstroms around the ion trajectory. The average lateral extension of these defects at the surface is much less than those of the bumps observed, thus they are not the dominant factor responsible for the bump formation on the HOPG surface.[16] On the other hand, the energy deposited into phonons is very condensed along the ion path as shown in Fig. 3(c), so we expect thermal spikes would be initiated according to the thermal spike model.[1,8,9,24,25]

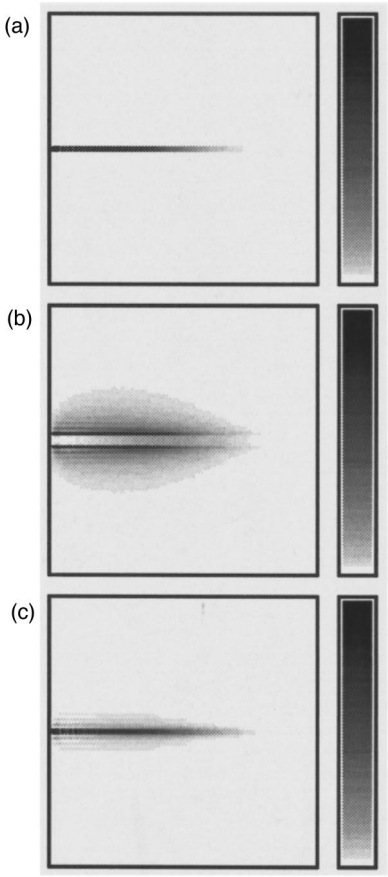

FIG. 2. 2D grey scale presentations for the average distribution of (a) vacancies, (b) interstitials and (c) phonons relative to a 3 keV Ar^+ ion trajectory in graphite. The lateral radius scale (vertical) is 50 Å with the ion trajectory at the centre. The depth scale (horizontal) is from 0 Å (left) to 100 Å (right). The grey scales (from bright to dark) are (a) 0–0.1 vacancy/Å^3, (b) 0–0.003 interstitial/Å^3, and (c) 0–1.5 eV/Å^3.

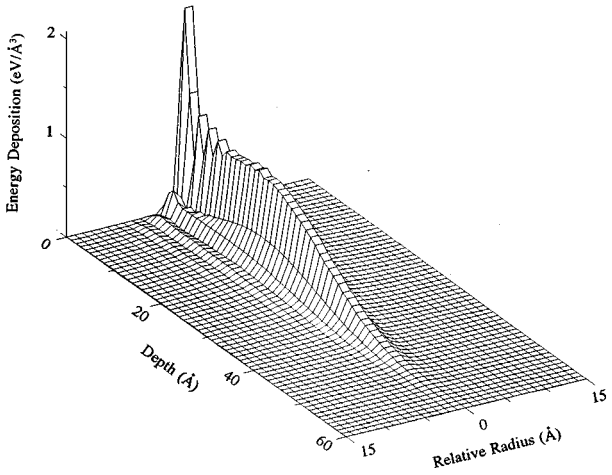

FIG. 3. The average deposited energy density $\varepsilon(r,x)$ relative to a 1.5 keV Ar_+ ion trajectory in graphite. The lateral radius is relative to the ion trajectory.

III. THERMAL SPIKE EFFECTS ON SURFACE DEFORMATION

The basic concept of thermal, or temperature, spikes was described by Seitz and Koehler.[1] A portion of the energy transmitted to the lattice by an incident particle can appear in the form of lattice vibrations concentrated locally so that the temperature would be sufficiently high to induce permanent rearrangement of the atoms of the solid. The spike is initiated by energy deposited in ion-atom and atom-atom collisions during the ballistic phase of the cascade, typically of subpicosecond duration. The majority of atoms in the spike are in motion, and the energy is then dissipated over picosecond time intervals in low-energy interactions. In other words, the thermal spike is formed in the region where the deposited energy density exceeds a threshold value ε_c, otherwise the spike effect will be much less pronounced.[1,8,9,24] The threshold ε_c in terms of the deposited energy per target atom is of the order of the lattice binding energy.[9,24] The formation of the thermal spike is complete within the time period of ballistic collision process (typically subpicosecond) whilst the spike phase may last for several picoseconds.[24] Therefore, Monte Carlo simulations or analytical methods based on the binary-collision approximation have been used to provide input for the starting point of thermal spikes in the cases where the binary-collision model is suitable.[8,9,24,25] The total energy deposited into the spike can be determined by

$$E_s = \int_{\varepsilon \geqslant \varepsilon_c} \varepsilon(r,x)\,dV, \tag{1}$$

where $\varepsilon(r,x)$ is the deposited energy density. The relative radius r is defined as the radial distance from the ion trajectory in the plane perpendicular to the depth scale x.

The formation of the spike is within the time period for the ballistic process to complete. The evolution of the spike phase involves additional processes. During the evolution of the spike, its energy spreads creating a expanded hot zone. According to the heat diffusion behavior of the thermal spike,[1] it is convenient to assume that the temperature (energy) is constant within the hot zone and drops to the ambient value at the boundary. From energy conservation, one obtains the volume of the hot zone as

$$V_m = \frac{l}{n_0}\frac{E_s}{Q_m^s}, \tag{2}$$

where Q_m^s is the average energy per atom in the hot zone, n_0 is the atomic density of the unirradiated target.

The deformation mechanism near surfaces can be very much different in character than in the interior of the target,[21] since the surface provides the place where anisotropic effects occur. The atoms in the heated zone of the spike exert a pressure on the surrounding medium. The pattern of dislocations produced near the hot zone will be such as to form a region of low density at the hottest regions and to compress the lattice in the cooler regions. The further development of the cascade involves the heat spreads outward creating a expanded hot zone. The initially displaced atoms may be reabsorbed in the hot zone. Since the pressure at the surface is zero, the internal high pressure developed in the hot zone pushes the activated atoms towards the surface giving rise to volume expansion of the hot zone, while the heat wave continues to spread outwards and the pressure in the expanding hot zone decreases. Finally the local temperature and internal pressure of the hot zone drop substantially where the cooling and resolidification processes take place. Depending upon the surface properties, the local structure of the deformed region and sputtering effects, craters or bumps may be formed on the surface. The evolution of the thermal spike occurs in a microscopic region, the concept of melting or liquid flow may not be appropriate. In this highly nonequilibrium state, additional processes occur, presumably thermal-dynamic and kinetic effects, atom migration and clustering, etc., which lead to certain local phase transformation. Since the spikes formed near the surface may contribute significantly to the deformation on the surface, an effective depth x_c is introduced to account for the spike effects on the surface.[28] Therefore, the effective spike energy contributed to the deformation on the surface can be obtained by

$$E_{\text{eff}} = \int_{\substack{\varepsilon \geqslant \varepsilon_c \\ x \leqslant x_c}} \varepsilon(r,x)\,dV. \tag{3}$$

This energy is confined in a volume of

$$V_{\text{eff}} = \int_{\substack{\varepsilon \geqslant \varepsilon_c \\ x \leqslant x_c}} dV. \tag{4}$$

These approximations for surface effects corresponding to ε_c and x_c have been discussed independently in the studies of sputtering[9] and surface damage.[16]

Generally, the shape of a spike is not purely cylindrical or spherical. In the case of low-energy ion bombardment of the HOPG surface, the cylindrical spike is a good approximation as discussed in the next section. The spike cylinder spreads laterally creating a hot cylinder. Similar to Eq. (2), one obtains the volume of the hot cylinder within the effective depth as

$$V_m' = \frac{1}{n_0}\frac{E_{\text{eff}}}{Q_m}. \tag{5}$$

TABLE I. Parameters for thermal spikes and bump formation due to low-energy single-ion impacts of HOPG surface.

Ion	Energy (keV)	Angle to surface	V_{pump} (Å^3)	δV_{pump} (Å^3)	E_{eff} (eV)	V_{eff} (Å^3)	Q_{eff} (eV/atom)	$dE/dx\|_{x<10\ \text{Å}}$ (eV/Å)
Ar	0.5	90	7230[a]	70(2)	139	27.1	5.1	20.8
Ar	1.5	20	8400[a]	400(2)	169	37.8	4.5	73.0
Ar	1.5	45	5600[a]	900(2)	113	22.4	5.0	32.2
Ar	1.5	90	4380[a]	(1)	73.7	13.9	5.3	20.7
Ar	3	90	3400[a]	600(4)	51.3	7.5	6.9	19.4
Ar	20	90	1500[b]		25.2	4.3	5.9	13.5
Xe	20	90	2760[b]		49.3	9.3	5.3	31.3
N	20	90	660[b]		8.7	3.9	2.2	4.2

[a]From Ref. 16 and updated as described in the text.
[b]Reference 14.

The activated atoms in this effective hot volume are forced by the internal high pressure towards the surface during the lateral expansion and cooling of the hot cylinder, inducing deformation on the surface. In the case of low-energy ion bombardment of the HOPG surface, where no significant sputtering occurs, one would expect a monotonic relationship between the bump volume and the effective spike energy if the spike effects dominate. If we assume the atomic density is n_m in the local deformed zone in which each atom receives the energy of Q_m, the difference between n_m and n_0 results in the final surface deformation after cooling and resolidification. The bump volume formed on the surface can be obtained as

$$V_{\text{bump}}=\frac{n_0-n_m}{n_m}\,V_m' = \frac{n_0-n_m}{n_m}\,\frac{1}{n_0}\,\frac{E_{\text{eff}}}{Q_m}. \tag{6}$$

The parameter Q_m is the average energy per atom in the expanded hot zone when the substantial cooling and resolidification processes begin. Since the processes take place at the surface where no external pressure is applied, Q_m is related to a threshold energy for structural deformation which depends upon target properties. So the difference in n_0 and n_m results in the bump volume on the surface. One would expect a linear relationship between the bump volume and the effective spike energy from Eq. (6). Such a dependence can be verified by applying the above model in the case of bump formation on HOPG surface due to low-energy single-ion impacts.

IV. BUMPS ON HOPG SURFACE DUE TO SINGLE-ION IMPACTS

The typical STM studies for the bump formation on HOPG surface due to low-energy single-ion bombardment can be found in previous articles.[11–16] The most suitable parameter related to this surface damage is the bump volume as discussed,[16] where the dependence of the bump volume on ion energy and incident angle has been studied systematically. The dependence of the average bump volume on ion species can be found.[14] The results are summarized in Table I. In the STM studies for 0.5–3 keV Ar^+ bombardment,[16] the bump volume calculated as the average of 200 bumps in each case. Several measurements were repeated in some cases, with the number of repeated measurements listed in the bracket of δV_{bump} column. The value V_{bump} is the average bump volume over several measurements, and δV_{bump} is the maximum deviation from the average value among different measurements. In order to evaluate the bump volume due to the thermal spikes, one need to consider the possibility for the formation of thermal spikes and their effects on the surface. The deposited energy profile $\varepsilon(r,x)$ due to single-ion impacts can be obtained using the Monte Carlo method described above. For example, the energy profiles for 3 and 1.5 keV Ar^+ bombardment of graphite at normal incidence to the surface are shown in Fig. 2(c) and Fig. 3, respectively. Such a profile of energy is deposited within subpicosecond duration of the ballistic collision process, thus it serves as the starting point for the formation of thermal spikes. For all the cases listed in Table I, the deposited energy is very concentrated along the ion trajectory showing a cylindrical distribution relative to the ion path. Since such a cylindrical character is an average behavior based on many trajectories, one would expect more elongated bumps to appear on the surface as the incident angle to the surface reduces. This is indeed observed as shown in Fig. 4, where the elongated bumps are marked with rectangles.

Based on the TRIM3D simulation results for the energy density $\varepsilon(r,x)$, the effective spike energy can be calculated using Eq. (3) where ε_c and x_c are adjustable parameters. In the cases of tilt angle incidence, the integration depth can be approximated by $x_c/\sin\alpha$ (where α is the angle of incidence to the surface). This is because that the lateral deflection of the ion paths near the surface is negligible as shown in Fig. 1, thus the ion path can be approximated by a straight line in the near-surface region. The purpose by adjusting ε_c and x_c is to obtain a monotonic relationship between V_{bump} and E_{eff} simultaneously for all the available data listed in Table I. As a result, we can only find a linear relationship around $x_c=16$ Å and $\varepsilon_c=0.25$ eV/Å^3 as shown in Fig. 5, while no other kinds of monotonic relationship can be adjusted obviously. This is in agreement with the linear dependence of Eq. (6), which suggests that thermal spikes formed in the near-surface region are responsible for the bump formation on HOPG surface due to single-ion impacts in the cases of current study. With $x_c=16$ Å and $\varepsilon_c=0.25$ eV/Å^3, the resulted

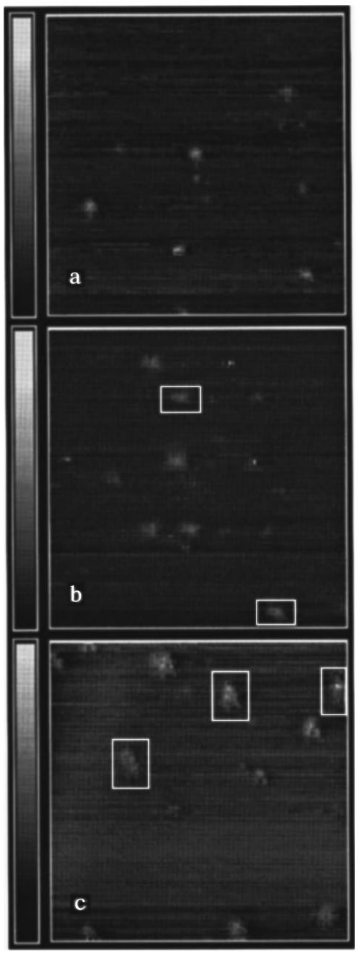

FIG. 4. STM images of the bumps on HOPG surfaces due to 1.5 keV Ar^+ bombardment at (a) 90°; (b) 45°, and (c) 20° incidence to the surface. The scan areas are 600×600 Å^2, and the grey scales (from dark to bright) are (a) 0–10 Å; (b) 0–10 Å; (c) 0–13 Å. The rectangles are drawn to highlight the elongated bumps.

values for the effective spike energy E_{eff} the effective spike volume V_{eff} and the average energy per atom in this volume, $Q_{\text{eff}}=E_{\text{eff}}/n_0V_{\text{eff}}$ are calculated and listed in Table I.

V. DISCUSSION

The parameter $x_c=16$ Å is consistent with the average radius (10–30 Å) of the bumps observed on HOPG surfaces.[14,16] Such an effective depth corresponds to 4–5 atomic layers of the surface. Due to the large interlayer spacing of graphite,[29] the dislocations below this depth may have less influence on the surface. Thus the assumption that only the spikes within an effective depth x_c contribute to the surface damage is a reasonable approximation. The threshold energy density for spike formation, $\varepsilon_c=0.25$ eV/Å^3, corresponds to 2.2 eV/atom for graphite. As expected for spike formation,[9,24] this threshold is of the order of the atomic binding energy of graphite, ~2 eV.[4] This energy corresponds to a temperature many times the melting point (3500 K) of graphite, hence large structural changes would be initiated by the spikes. In the case of heavy ion bombardment of metals, local melting and liquid flow onto the surface are suggested in recent MD simulation studies.[21] However, the efficiency

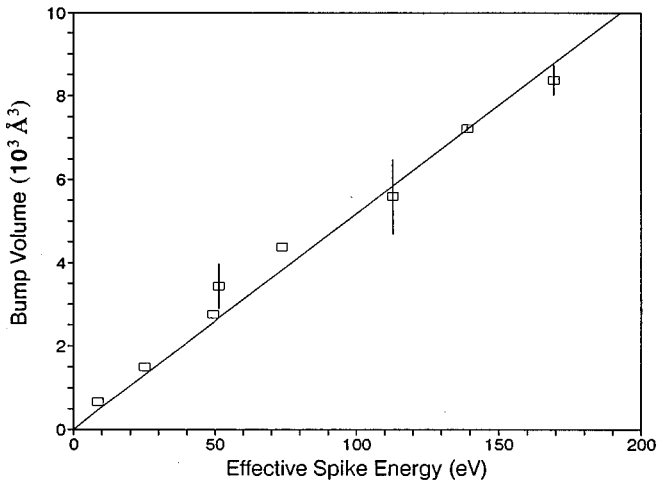

FIG. 5. The relationship between the observed bump volume and the effective spike energy (with $x_c=16$ Å and $\varepsilon_c=0.25$ eV/Å^3) of graphite due to single-ion impacts. The data points with available error bars are listed in Table I. The straight line is a least-squares fit to the data.

of such processes should depend on target properties such as the melting point,[18] surface binding energy and target structures. In the thermal spike model, the average temperature in the hot zone may drop below the melting point while deformation still occurs. For graphite, with an energy of $Q_m\approx0.1$ eV/atom, the estimated lateral extension of the spikes agrees well with the average bump diameter observed by STM.[16] This Q_m value corresponds to a temperature (~1200 K), which suggests that structural deformation of HOPG takes place at temperatures well below the melting point (3500 K). From the slope of Fig. 5 (~52.6 Å^3/eV) and $Q_m=0.1$ eV/atom, one obtains $n_m/n_0\approx65\%$ according to Eq. (6), which corresponds to a local density of ~1.5 g/cm^3 well below the HOPG bulk density 2.26 g/cm^3. This low density agrees well with the typical densities of various forms of carbon or graphite (1.4–1.9 g/cm^3),[31,32] which suggests local structural deformation and expansion due to single-ion impacts. The observed bump heights of 2–4 Å correspond to expansions of 15–30 % of the effective depth x_c (16 Å), while lateral expansions in the basal plane are expected to be less pronounced in graphite due to its layered structure.[29] Such levels of expansion are also consistent with that observed in neutron-irradiated graphite.[29]

The thermal spike model above also agrees with the STM results that each bump corresponds to a single-ion impacts (1:1 ratio) in the cases listed in Table I. The value $Q_{\text{eff}}=2.2$ eV/atom for 20 keV N^+ bombardment is just about the threshold energy for spike formation in graphite, thus spike effects are also expected as shown in Fig. 5. This is different from previous discussion.[16] In the case of 20 keV C^+ bombardment of HOPG, it has been found that the number of bumps observed is less than that of ion impacts.[13] This can be understood as that spikes may not be formed in every C impact statistically since lower energy density deposited along the ion track is expected. It should be pointed out that the above results are based on the modified Monte Carlo TRIM simulation, which does not take into account the crystalline structure of HOPG. This problem could be overcome

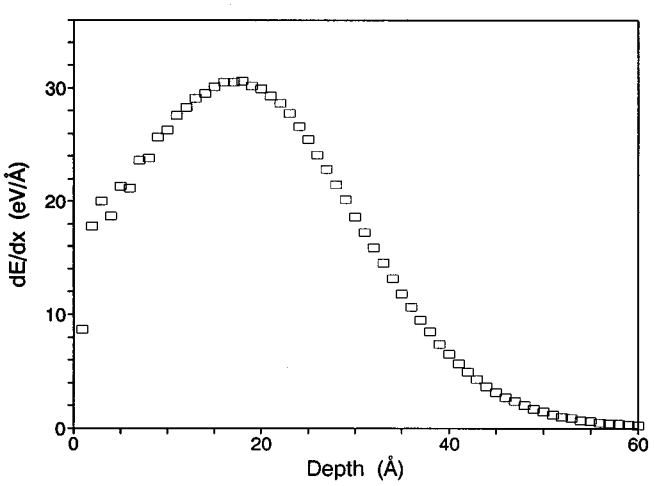

FIG. 6. One-dimensional energy deposition rate dE/dx as a function of depth for 1.5 keV Ar^+ in graphite.

by using the MARLOWE code.[7] However, for the statistical results in the STM studies,[14,16] no specific channeling effects are measured in the ion bombardment of HOPG surfaces. Although MD simulations can provide more detailed information for the dynamic processes, it is not practical so far to provide sufficient statistical information due to lack of suitable interaction potentials and limitation of computation time.[21,22] It is accepted that Monte Carlo simulations or analytical methods provide reasonable approximation for the statistical profile of energy deposition during the ballistic collision process,[9,24,25] thus this study demonstrates the statistical generality of thermal spike effects in low-energy ion bombardment of solid surfaces.

Normally, the average nuclear energy loss (dE/dx) has been used in describing the nonlinear behavior due to spike effects. However, such a one-dimensional parameter may not be suitable in the studies related to spike effects. This is because the spike formation relates to the energy density which is a three-dimensional term. For example, the one-dimensional energy deposition rate dE/dx as a function of depth, as shown in Fig. 6, is obtained by integrating the energy density laterally without the threshold condition $\varepsilon > \varepsilon_c$. The difference between $\varepsilon(r,x)$ and dE/dx is obvious as shown in Figs. 3 and 6 especially in the near-surface region. The energy density $\varepsilon(r,x)$ is maximum close to the impact point just below the surface, while the dE/dx is relatively low at the surface. For comparison, the average dE/dx in the near-surface region (within 10 Å below the surface) for each case is listed in Table I. It is found that the average bump volume does not scale monotonically with the (dE/dx) term. On the other hand, it would be necessary to choose a critical parameter associated with the spike formation, such as the effective energy E_{eff} as described in Eq. (2). As expected, the bump volume scales linearly with the effective spike energy in the near-surface region with reasonable approximations corresponding to ε_c and x_c. This is consistent with the conclusion that the mean energy loss is not sufficient for a treatment of the nonlinear effects.[9]

VI. SUMMARY

It is demonstrated that Monte Carlo simulations can provide useful results as the starting point for the formation of thermal spikes during the ballistic collision process. The thermal spike model agrees well with the STM results for the bump formation on HOPG surfaces due to low-energy single-ion impacts. It is suggested that the one-dimensional energy deposition rate dE/dx is not suitable to describe the spike effects. On the other hand, a three-dimensional parameter corresponding to the nature of spike formation, such as the effective spike energy E_{eff}, should be used. Detailed MD simulations and more experimental data are needed to further verify the model presented in this work.

ACKNOWLEDGMENTS

The authors would like to thank Dr. S. Prawer for the inspiration about the single-ion impacts and Associate Professor D. J. O'Connor and G. Cotterill for their kind help. Financial support from the Australian Research Council is acknowledged, without which this study would be impossible.

*Present address: Department of Radiology, The University of Melbourne, Royal Melbourne Hospital, Vic. 3050, Australia. Fax No. 61-3-9342 8369; Electronic address: QY@radior.medrmh.unimelb.edu.au

[1] F. Seitz and J. S. Koehler, Solid State Physics: *Advances in Research and Applications*, edited by F. Seitz and D. Turnbull (Academic, New York, 1956), Vol. 2, p. 305.

[2] J. A. Brinkman, J. Appl. Phys. **25**, 961 (1954); Am. J. Phys. **24**, 246 (1956).

[3] G. Carter and D. G. Armour, Thin Solid Films **80**, 13 (1981).

[4] J. F. Ziegler, J. P. Biersack, and U. Littmark, *The Stopping and Range of Ion in Solids* (Pergamon, New York, 1985).

[5] W. Eckstein, *Computer Simulation of Ion-Solid Interactions* (Springer-Verlag, Berlin, 1991).

[6] R. Smith and R. P. Webb, Nucl. Instrum. Methods Phys. Res. Sect. B **67**, 373 (1992).

[7] M. T. Robinson and I. M. Torrens, Phys. Rev. B **9**, 5008 (1974).

[8] P. Sigmund, Nucl. Instrum. Methods Phys. Res. Sect. B **27**, 1 (1987), and references therein.

[9] I. S. Bitensky, Nucl. Instrum. Methods Phys. Res. Sect. B **83**, 110 (1993); **88**, 69 (1994).

[10] I. H. Wilson, N. J. Zheng, U. Knipping, and I. S. T. Tsong, Phys. Rev. B **38**, 8444 (1988); Appl. Phys. Lett. **53**, 2039 (1988); J. Vac. Sci. Technol. A **7**, 2840 (1989).

[11] L. Porte, M. Phaner, C. H. de Villeneuve, N. Moncoffre, and J. Tousset, Nucl. Instrum. Methods Phys. Res. Sect. B **44**, 116 (1989).

[12] L. Porte, C. H. de Villeneuve, and M. Phaner, J. Vac. Sci. Technol. B **9**, 1064 (1991).

[13] R. Coratger, A. Claverie, F. Ajustron, and J. Beauvillain, Surf. Sci. **227**, 7 (1990).

[14] R. Coratger, A. Claverie, A. Chahboun, V. Landry, F. Ajustron, and J. Beauvillain, Surf. Sci. **262**, 208 (1992).

[15] H. Kang, K. H. Park, C. Kim, B. S. Shim, S. Kim, and D. W.

Moon, Nucl. Instrum. Methods Phys. Res. Sect. B **67**, 312 (1992).
[16] T. Li, B. V. King, R. J. MacDonald, G. F. Cotterill, D. J. O'Connor, and Q. Yang, Surf. Sci. **312**, 399 (1994).
[17] R. P. Webb and D. E. Harrison, Jr., Phys. Rev. Lett. **50**, 1478 (1984).
[18] R. S. Averback, T. Diaz de la Rubia, H. Hsieh, and R. Benedek, Nucl. Instrum. Methods Phys. Res. Sect. B **59/60**, 709 (1991).
[19] H. M. Urbassek and K. T. Waldeer, Phys. Rev. Lett. **67**, 105 (1991).
[20] V. G. Kapinos and D. J. Bacon, Philos. Mag. A **68**, 1165 (1993).
[21] Mai Ghaly and R. S. Averback, Phys. Rev. Lett. **72**, 364 (1994); R. S. Averback and Mai Ghaly, Nucl. Instrum. Methods Phys. Res. Sect. B **90**, 191 (1994).
[22] A. Gras-Martí, R. Smith, K. Beardmore, J. J. Jiménez-Rodríguez, V. Konoplev, and J. Ferrón (unpublished).
[23] A. M. C. Pérez-Martín, J. Domínguez-Vázquez, J. J. Jiménez-Rodríguez, R. Collins, and A. Gras-Martí, J. Phys. Condens. Matter **5**, A257 (1993); Nucl. Instrum. Methods Phys. Res. Sect. B **90**, 424 (1994).
[24] P. Sigmund, Appl. Phys. Lett. **25**, 169 (1974); **27**, 52 (1975).
[25] M. Alurralde, A. Caro, and M. Victoria, J. Nucl. Mater. **183**, 33 (1991).
[26] Electronic straggling is added for all ions in TRIM92.13 and later versions, which is defined as the minimum of Firsov or Bohr values [see Eq. (4-32) in Ref. 4]. The previous versions only include electronic straggling for H, He, and Li ions. The current TRIM3D code uses the universal empirical formula Refs. 27 and 28.
[27] Q. Yang, D. J. O'Connor, and Zhonglie Wang, Nucl. Instrum. Methods Phys. Res. Sect. B **61**, 149 (1991).
[28] Q. Yang and R. J. MacDonald, Nucl. Instrum. Methods Phys. Res. Sect. B **83**, 303 (1993).
[29] B. T. Kelly, *Physics of Graphite* (Applied Science, London, 1981).
[30] H. J. Steffen, D. Marton, and J. W. Rabalais, Phys. Rev. Lett. **68**, 1726 (1992); H. J. Steffen, D. Marton and J. W. Rabalais, Nucl. Instrum. Methods Phys. Res. Sect. B **67**, 308 (1992).
[31] H. W. Davidson, P. K. C. Wiggs, A. H. Churchouse, F. A. P. Maggs, and R. S. Bradley, *Manufactured Carbon* (Pergamon, London, 1968), p. 60.
[32] C. L. Mantell, *Carbon and Graphite Handbook* (Wiley, New York, 1968).